Colorectal tumors require NUAK1 for protection from oxidative stress

Jennifer Port[#1], **Nathiya Muthalagu**[#2], **Meera Raja**[1], **Fatih Ceteci**[2], **Tiziana Monteverde**[1], **Bjorn Kruspig**[1], **Ann Hedley**[2], **Gabriela Kalna**[2], **Sergio Lilla**[2], **Lisa Neilson**[2], **Martina Brucoli**[1], **Katarina Gyuraszova**[1], **Jacqueline Tait-Mulder**[1], **Mokdad Mezna**[3], **Silvija Svambaryte**[1], **Amy Bryson**[1], **David Sumpton**[2], **Allan McVie**[1], **Colin Nixon**[2], **Martin Drysdale**[3], **Hiroyasu Esumi**[4], **Graeme I. Murray**[5], **Owen J. Sansom**[1,2], **Sara R. Zanivan**[1,2], and **Daniel J. Murphy**[1,2,§]

[1]Institute of Cancer Sciences, University of Glasgow, UK

[2]CRUK Beatson Institute, Garscube Estate, Switchback Rd. Glasgow, G61 1BD

[3]Drug Discovery Unit, CRUK Beatson Institute, Glasgow, UK

[4]National Cancer Center Hospital, Kashiwa, Chiba, Japan

[5]Dept. of Pathology, University of Aberdeen, UK

[#] These authors contributed equally to this work.

Abstract

Exploiting oxidative stress has recently emerged as a plausible strategy for treatment of human Cancer and anti-oxidant defences are implicated in resistance to chemo- and radiotherapy. Targeted suppression of anti-oxidant defences could thus broadly improve therapeutic outcomes. Here we identify the AMPK-related kinase NUAK1 as a key component of the anti-oxidant stress response pathway and reveal a specific requirement for this role of NUAK1 in colorectal cancer. We show that NUAK1 is activated by oxidative stress and that this activation is required to facilitate nuclear import of the anti-oxidant master regulator NRF2: Activation of NUAK1 coordinates PP1β inhibition with AKT activation in order to suppress GSK3β-dependent inhibition of NRF2 nuclear import. Deletion of NUAK1 suppresses formation of colorectal tumors, while acute depletion of NUAK1 induces regression of pre-existing autochthonous tumors. Importantly, elevated expression of NUAK1 in human colorectal cancer is associated with more aggressive disease and reduced overall survival.

Keywords

[§]To whom correspondence should be addressed: daniel.murphy@glasgow.ac.uk, Phone: +44 141 330 8710.

Introduction

The relentless drive to proliferate exposes tumor cells to considerable metabolic stress. Proliferating tumor cells increase nutrient consumption in order to balance the competing demands of macromolecular synthesis, towards which a large proportion of nutrient metabolites are diverted, with the energetic cost of sustaining viability, measured in ATP (1). Increased metabolic activity elevates production of reactive oxygen species (ROS), altering signal transduction and, at very high levels, inflicting damage upon lipids, proteins and nucleic acids (2). In the context of a growing solid tumor with ineffective vascularity, tumor cells are commonly deprived of their preferred nutrients and exposed to hypoxia, which also increases ROS production, adding cell-extrinsic sources of further metabolic stress. In order to survive such stress, tumor cells must adapt flexibly and continuously by modulating their rates of macromolecular synthesis, cell growth, and proliferation, in order to maintain ATP homeostasis and counteract ROS. Failure to do so leads to ATP collapse, toxic levels of ROS, and loss of viability. As such, targeted suppression of adaptive measures used by tumor cells to counteract metabolic stress may yield therapeutic benefit in cancer treatment.

NUAK1 (aka ARK5) is one of 12 kinases related by sequence homology to the catalytic α subunits of AMPK (3). Collectively, these kinase play various roles in regulating cell adhesion and polarity, cellular and organismal metabolism, and in the cellular response to various forms of stress, including oxidative, osmotic and energetic stress (4, 5). NUAK1 is a common target of several miRNAs that are frequently suppressed in cancer, suggesting a potential role for NUAK1 in tumorigenesis (6–8). Accordingly, we previously reported that NUAK1 is required to sustain viability of cancer cells when MYC is overexpressed (9).

In contrast with the widely studied AMPK, the molecular targets and downstream pathways governed by NUAK1 are poorly defined. To date, the best-characterized substrate of NUAK1 is the PP1β subunit, MYPT1 (PPP1R12A). During cell detachment, phosphorylation of MYPT1 by NUAK1 inhibits PP1β phosphatase activity towards myosin light chain. Inhibition of NUAK1 thus increases PP1β activity, delaying cell detachment and suppressing cell migration (10). Other work points to a role for NUAK1 in metabolic regulation. Muscle-specific deletion of *Nuak1* protects mice from high fat diet-induced diabetes, attributable to increased glucose uptake and increased conversion of glucose to glycogen by Nuak1-deficient skeletal muscle (11). An earlier study showed that NUAK1 protects cancer cells from nutrient deprivation-induced apoptosis (12). In the context of MYC overexpression, we showed that NUAK1 is required to maintain ATP homeostasis, in part by facilitating AMPK-dependent inhibition of TORC1-driven macromolecular synthesis (9, 13). Failure to engage this checkpoint results in cell death under conditions of metabolic stress (14–16).

Our previous work thus suggested that NUAK1 may present a good target for therapy, specifically in the context of MYC-driven cancers. Human colorectal cancer (CRC) is uniformly characterized by deregulated expression of MYC and mouse models have shown that expression of endogenous *Myc* is required for intestinal polyp formation upon loss of *Apc*, the most common tumor-initiating event in human CRC (17, 18). We asked therefore if NUAK1 is required to support tumor cell viability in CRC. Here we show that *NUAK1* is

overexpressed in human CRC and that high *NUAK1* expression correlates with reduced overall survival. Using genetically engineered mouse models of CRC driven by sporadic loss of *Apc*, we show that NUAK1 is required for both initiation and maintenance of autochthonous colorectal tumors. NUAK1 facilitates nuclear translocation of the anti-oxidant master regulator NRF2 by counteracting negative regulation of NRF2 by GSK3β. Depletion or inhibition of NUAK1 thus renders human CRC cells and murine colorectal tumors vulnerable to oxidative stress-induced cell death. Our data reveal NUAK1 as a candidate therapeutic target in human CRC.

Results

Nuak1 overexpression is associated with worse outcome in human CRC

We used RNA-Scope in situ hybridization to examine *NUAK1* expression in a 660-sample tissue microarray of human CRC (19). *NUAK1* is weakly expressed in normal human colonic epithelium but increased expression is significantly enriched in aggressive (Dukes' stage B & C) CRC (Fig. 1A & S1A, B). *In silico* examination of the TCGA Colorectal adenocarcinoma cohort similarly showed significantly elevated *NUAK1* expression in advanced (T stage 3 & 4) versus early (T stage 1 & 2) disease, and in patients with lymph node metastasis versus none (Fig. 1B). Meta-analysis of 17 independent cohorts comprising 947 human CRC samples, via SurvExpress (20), also revealed significantly higher *NUAK1* expression in the high versus low risk group, and elevated *NUAK1* expression was associated with significantly reduced overall survival and a hazard ratio of 1.49 (Fig. 1C, D). A similar reduction of overall survival was borne out by individual analysis of two large cohorts in which the outcome for the majority of patients was known (Fig. S1C-F) (21, 22). Elevated *NUAK1* expression thus correlates with worse outcome in colorectal cancer.

We therefore examined the functional requirement for NUAK1 in human CRC cell lines using 2 previously described highly-selective NUAK1 inhibitors, HTH-01-015 and WZ4003. HTH-01-015 is reported to show little-to-no activity towards AMPK or other related kinases while WZ4003 selectively inhibits both NUAK1 and the closely related NUAK2 (23). Overexpression of NUAK1 and NUAK2 in human CRC tends to be mutually exclusive and accordingly we detected a reciprocal pattern of NUAK protein expression in CRC cell lines (Fig. S1G, H). Treatment with 5μM HTH-01-015 suppressed proliferation of multiple cell lines and this effect was reproduced by RNAi-mediated depletion of NUAK1 (Fig. S1I-L). Strikingly, treatment with 10μM HTH-01-015 was profoundly toxic in the same cell lines and correlated with a stronger reduction in phosphorylation of the NUAK1/NUAK2 substrate, MYPT1, even in cells that express very low levels of NUAK1 (Fig. 1E, F). This cytotoxic effect was also observed using the dual NUAK inhibitor WZ4003, suggesting it reflects on-target activity of the inhibitors. Notably, WZ4003 gave greater suppression of p-MYPT1[S445], consistent with dual inhibition of NUAK1 and NUAK2, and showed somewhat greater potency, driving significant cell death at 5μM in SW480 cells (Fig. S1M, N). Inhibition of NUAK1 is thus sufficient to drive apoptosis in CRC cells and death does not require complete suppression of MYPT1[S445] phosphorylation. In contrast with the CRC lines, wild-type MEFs and U2OS cells were comparatively resistant to both inhibitors, especially to the NUAK1-selectve HTH-01-015 (Fig.1G & S1O, P), consistent with previous

data showing that U2OS are refractory to NUAK1 depletion (9). Notably, both inhibitors completely suppressed MYPT1 phosphorylation in U2OS, indicating that NUAK1 accounts for the vast majority of MYPT1^{S445} phosphorylation in this cell type. As we showed previously in MEFs (5), overexpression of MYC strongly sensitized U2OS to HTH-01-015-induced apoptosis (Fig. 1H). Conversely, depletion of endogenous MYC rescued CRC cells from HTH-01-015-induced apoptosis and rescue was proportional to the degree of MYC depletion, consistent with an ectopic requirement for NUAK1 in cells with deregulated MYC (Fig. 1I).

Nuak1 is required for formation of colonic polyps in mice

In order to investigate the *in vivo* requirement for *NUAK1* in CRC, we bred mice bearing a floxed *Nuak1* allele (*Nuak1$^{FL/FL}$*) (11) onto a Tamoxifen (Tam)-inducible mouse model of sporadic intestinal cancer: <u>*Villin-CreER^{T2}*</u>; <u>*APC$^{FL/+}$*</u>;*lsl-<u>K</u>Ras^{G12D}* (VAK for short). In this model, transient Tam-dependent activation of CreER^{T2} in the intestines of adult mice drives widespread deletion of one copy of *Apc* simultaneous with expression of oncogenic KRas^{G12D}, however, tumor formation requires stochastic loss of the second copy of *Apc* (Fig. S2A). In the absence of mutant KRas, *Apc* null polyps are largely restricted to the small intestine, whereas in the presence of mutant KRas, adenomas form in both large and small intestine (19).

Using a single injection of Tam to transiently activate CreER^{T2}, we deleted *Nuak1* in the intestines of adult <u>*Villin-CreER^{T2}*</u>; <u>*APC$^{FL/+}$*</u>;*lsl-<u>K</u>Ras^{G12D}*;<u>*Nuak1$^{FL/FL}$*</u> mice (VAKN for short) and aged mice until symptomatic in order to compare the intestinal tumor burden with that of symptomatic VAK mice. Deletion of *Nuak1* profoundly suppressed both the number and size of individual tumors in the colon of VAKN mice, compared to VAK controls (Fig. 2A-D). In contrast, we observed no significant difference in either the number or size of tumors that arose in the small intestine (SI), and VAKN mice required sacrifice concurrently with VAK mice (Fig. S2B-D). However, Q-PCR analysis of *Nuak1* expression in individual polyps harvested from the SI of VAKN mice revealed enrichment of *Nuak1* mRNA when compared with disease-free adjacent tissue (Fig. S1E), indicating a failure of transient CreER activation to efficiently delete *Nuak1* in the tumor initiating population of the small intestine. The absence of a *Nuak1$^{FL/FL}$* phenotype in SI tumors thus appears to reflect technical failure but is of little clinical relevance given the rarity of SI tumors in human populations. Colonic tumors in VAKN mice presented with comparable levels of nuclear β-Catenin and sporadic phospho-Erk1/2 staining, as compared with VAK tumors (Fig. S2F), however, all tumors arising in VAKN mice retained detectable expression of *Nuak1* mRNA (see Fig. S2G for examples), suggesting a selective pressure to retain Nuak1 in colonic tumor epithelium. Importantly, deletion of *Nuak1* in otherwise wild-type mice had no apparent effect on small or large intestine architecture or function (Fig. S3A-C), suggesting that the requirement for Nuak1 in the adult gut is restricted to transformed tissue.

Nuak1 activity is required for *ex-vivo* spheroid formation

Homozygous deletion of *Apc* (A^{Hom}) in the gut rapidly gives rise to a Myc-dependent "crypt progenitor" phenotype, characterized by an extension of the transit-amplifying population into the normally quiescent villi of the small intestine (17). This phenotype was unimpaired

by deletion of *Nuak1* in VA[Hom]N intestines (Fig. S3D). VA[Hom]K transformed gut epithelium gives rise to spheroids when cultured in 3D *ex vivo*, reflecting the tumor-initiating capacity of the transformed tissue (24). Primary VA[Hom]KN colonic epithelium showed reduced spheroid-generating capacity, compared to VA[Hom]K epithelium (Fig. 2E & F). Nuak1 expression was clearly detectable in the few VA[Hom]KN spheroids that grew, suggesting that they likely arose from cells that escaped Cre-mediated *Nuak1* deletion (Fig. 2G). Interestingly, a similar reduction in spheroid-generating capacity was also observed in primary epithelium isolated from the small intestine (Fig. 2E & F). Accordingly, pharmacological inhibition of Nuak1 with either HTH-01-015 or WZ4003 profoundly suppressed formation of spheroids by VA[Hom]K gut epithelium from both small and large intestine (Fig. 2H & I), whereas wild-type organoids were refractory to treatment over the same time frame (Fig. S3E).

NUAK1 regulates the NRF2-dependent oxidative stress response

Reasoning that key physiological roles of NUAK1 would be conserved across cell types, we exploited the fact that U2OS cells are refractory to NUAK1 suppression (in the absence of MYC overexpression) and express very little NUAK2, and performed an unbiased transcriptomic analysis after RNAi-mediated depletion of NUAK1. Metacore GeneGO pathway analysis revealed regulation of cholesterol synthesis, cell adhesion, and glutathione metabolism amongst the topmost pathways modulated upon NUAK1 depletion (Fig. 3A). The role of NUAK1 in regulating cell adhesion via phosphorylation of MYPT1 was described previously (10), while the modulation of glutathione metabolism suggested a novel role for NUAK1 in the anti-oxidant defense pathway. Strikingly, our transcriptomic analysis revealed a coordinated reduction in expression of a host of genes that are regulated by the anti-oxidant transcription factor NRF2 (*NFE2L2*) (25), including the catalytic and regulatory subunits of the Glutamate-Cysteine Ligase; ROS scavengers Thioredoxin, Peroxiredoxin and MGST; and Glutathione Reductase (Fig. 3B & S4A). Acute inhibition of NUAK1 in U2OS cells with HTH-01-015 recapitulated these results (Fig. 3C), as did CRE-mediated deletion of *Nuak1* in primary MEFs (Fig. S4B, C), confirming the conservation of this effect across cells types and species. RNA-SEQ analysis of SW480 CRC cells upon depletion of NUAK1 revealed a strong overlap with genes modulated upon depletion of NRF2 (*NFE2L2*), including several anti-oxidant pathway genes and the miR17-92 cluster, recently shown to negatively regulate LKB1 upstream of NUAK1 (26), suggestive of feedback regulation (Fig. 3D, E). Similar results were obtained in HCT116 cells (Fig. 3D). Pathway analysis showed broadly similar transcriptional effects of depletion of either NUAK1 or NRF2, while analysis of down-regulated genes revealed significant enrichment for pathways "Oxidative stress" and "NRF2 regulation of oxidative stress" in both instances (Table S1 & S2).

The reduced expression of NRF2 target genes suggested that NUAK1-deficient cells would be hypersensitive to oxidative stress. Accordingly, we detected elevated levels of cytosolic H_2O_2 in U2OS, multiple CRC cell lines, and VAK colonic spheroids, after acute treatment with HTH-01-015 (Fig. 3F-I), while depletion of NUAK1 sensitized U2OS and multiple CRC cell lines to H_2O_2-induced cell death, consistent with the inhibitor and RNAi each reducing anti-oxidant buffering capacity, albeit to different degrees (Fig. 3J). Similar

sensitization to H_2O_2-induced cell death was also observed upon CRE-mediated deletion of NUAK1 in MEFs, providing genetic confirmation of the specificity of this effect (Fig. S4D, E). CRC lines with lower levels of NUAK1 were inherently more sensitive to ROS-induced cell death, even in the absence of NUAK1 depletion, compared with cells expressing higher levels of NUAK1, while the relatively modest sensitization of SW480 cells compared with U2OS cells may reflect differences in the efficiency of NUAK1 depletion or indeed the relative expression of NUAK2. Notably, depletion of NUAK1 in some CRC lines resulted in increased NUAK2 expression (Fig. S1L). Importantly, provision of exogenous anti-oxidants significantly rescued human CRC cells (Fig. 3K & S4F) and VAK spheroids (Fig. 3L & S4G) from NUAK1 inhibitor-induced apoptosis, indicating that ROS contributes substantially to cell death in both settings. The remaining levels of cell death measured in the CRC cell lines likely reflects exhaustion of the exogenous anti-oxidant, evidenced by intermediate levels of ROS in cells treated for 8hrs with NUAK1 inhibitor in the presence of Trolox (Fig. S4H, I).

NUAK1 promotes nuclear translocation of NRF2 by antagonizing GSK3β

NRF2 was recently described to contain an AMPK-substrate consensus phospho-motif (27) that could potentially be targeted for phosphorylation by NUAK1. We used immunoprecipitation (IP) of Flag-tagged NRF2 followed by immunoblotting with a pan-phospho-AMPK-substrate antibody to assess the influence of NUAK1 inhibition on NRF2 phosphorylation levels but detected no difference (Fig. S5A). Similarly, purified NUAK1 showed no activity towards a corresponding NRF2 peptide *in-vitro* (Fig. S5B). Thus, NRF2 does not appear to be a direct target of NUAK1 kinase activity.

We noticed that acute inhibition of NUAK1 resulted in decreased total NRF2 levels (Fig. 4A). NRF2 is regulated by KEAP1, which sequesters NRF2 in the cytoplasm while targeting it continuously for Ubiquitin-dependent degradation (28, 29). We asked if KEAP1 is required for regulation of NRF2 by NUAK1. As expected, RNAi-mediated depletion of KEAP1 increased basal levels of NRF2, yet concomitant inhibition of NUAK1 continued to reduce total NRF2 protein levels (Fig. 4B). Accordingly, cyclohexamide time-course analysis showed that NUAK1 depletion reduces total NRF2 levels but does not affect the rate of NRF2 degradation, per se (Fig. S5C). KEAP1 contains a number of Cysteine residues that are subject to oxidation and, in the presence of ROS, oxidized KEAP1 releases NRF2 allowing it to translocate to the nucleus and activate transcription (30). We therefore examined NUAK1-depleted or HTH-01-015-treated U2OS cells for nuclear accumulation of NRF2 after acute treatment with H_2O_2 and found that loss of NUAK1 activity strongly suppressed ROS-induced nuclear accumulation of NRF2 (Fig. 4C). Accordingly, ROS-induced transcription of NRF2 targets was also suppressed upon depletion of NUAK1 (Fig. 4D). Analysis in multiple CRC cell lines likewise revealed that depletion of NUAK1 suppresses ROS-driven NRF2 nuclear accumulation, indicating that this role of NUAK1 is conserved in CRC (Fig. 4E & S5D). Additionally, this role of NUAK1 is at least partially shared with NUAK2, as depletion of NUAK2 in SW620 cells similarly suppressed peroxide-induced nuclear accumulation of NRF2 (Fig. S5E).

We used unbiased, SILAC-based phospho-proteomics to identify candidate mediators of NRF2 regulation upon acute inhibition of NUAK1 in U2OS cells (see schematic, Fig. S5F). Ser[445] of MYPT1 was the only site resident within a recognizable AMPK-related kinase consensus motif that was consistently reduced upon NUAK1 inhibition. This analysis also revealed reduced inhibitory phosphorylation of GSK3β at Ser[9] and a corresponding increase in phosphorylation of multiple GSK3β targets (Fig. 5A & Table S3). GSK3β is known to suppress nuclear accumulation of NRF2: In the presence of oxidative stress, activation of AKT inhibits GSK3β via Ser[9] phosphorylation, allowing nuclear accumulation of NRF2 (31). We therefore examined the influence of NUAK1 depletion on ROS-driven signal transduction via AKT and GSK3β. Treatment of U2OS cells with H_2O_2 rapidly activated AKT, leading to increased GSK3β[S9] phosphorylation. Upon depletion of NUAK1, activation of AKT by H_2O_2 was unimpaired, however, the inhibitory phosphorylation of GSK3β was strongly reduced, suggesting that NUAK1 may limit de-phosphorylation of GSK3β[S9] (Fig. 5B). Similar results were observed upon H_2O_2 treatment of NUAK1-depleted SW480 cells (Fig. 5C), while treatment with NUAK1 inhibitor suppressed GSK3β[S9] phosphorylation in SW480 cells and in VAK LI spheroids (Fig. 5D, E). Notably, phosphorylation of MYPT1 by NUAK1 inhibits PP1β activity (10) and PP1β was previously shown to dephosphorylate GSK3β (32, 33). Strikingly, H_2O_2 led to a clear increase in NUAK1-dependent MYPT1 phosphorylation (Fig. 5B), suggesting that ROS coordinately activates AKT and inactivates PP1β (via NUAK1) in order to suppress GSK3β activity. Significantly, inhibition of GSK3β stabilized total NRF2 levels and rescued nuclear accumulation of NRF2 in NUAK1-deficienct SW480 cells (Fig. 5F & S5G). Interestingly, depletion of PTEN similarly rescued nuclear NRF2, suggesting that the requirement for NUAK1 in this pathway can be overcome by strongly deregulated AKT signaling (Fig. S5H).

Regulation of NUAK1 by ROS and NRF2

We asked if NUAK1 is an integral part of the oxidative stress response pathway. Depletion of NRF2 with 2 independent siRNAs consistently reduced NUAK1 protein levels (Fig. 6A). Examination of the NUAK1 promoter revealed a near-consensus anti-oxidant response element (ARE) located approximately 1.2kb upstream of the NUAK1 transcription start site, and NRF2 chromatin IPs showed specific binding of NRF2 to the putative *NUAK1* ARE, albeit at much lower efficiency than to the canonical NRF2 target, *HMOX1* (Fig. 6B, C). Treatment of U2OS cells with H_2O_2 modestly increased NUAK1 mRNA but had much greater influence on NUAK1 protein, suggesting that post-translational regulation may have greater functional impact (Fig. 6D, E). Time-course analysis revealed that H_2O_2 treatment rapidly increased activating phosphorylation of NUAK1 at Thr211, and consequent MYPT1[S445] phosphorylation, downstream. These changes occur within the same time-frame as increased AKT phosphorylation, known to result from direct inactivation of PTEN by ROS (34), suggesting that ROS may directly modify NUAK1 (Fig. 6F). To investigate this hypothesis, we first used Dimedone labeling (35) of cells expressing FLAG-tagged NUAK1 to measure Cysteine oxidation after H_2O_2 treatment: Treatment with increasing doses of H_2O_2 resulted in increased Dimedone labeling of FLAG-immunoprecipitated NUAK1 (Fig. 6G). Consistently, MS analysis of Iodo-acetamide labeling of FLAG-NUAK1 IPs from cells treated for 5 minutes with H_2O_2 similarly revealed increased oxidation of multiple NUAK1 Cysteines, as compared with untreated controls (Fig. 6H). Collectively, our data suggest a

model wherein ROS-dependent activation of NUAK1 coordinates inhibition of PP1β with activation of AKT in order to counteract suppression of nuclear NRF2 by GSK3β (Fig. 6I).

Modeling the therapeutic potential of Nuak1 suppression *in vivo*

The above data collectively suggest that NUAK1 may be an excellent target for therapeutic intervention in CRC. However, the relatively poor potency of the NUAK1 inhibitors used above preclude their use *in vivo*. We therefor employed a doxycycline-inducible RNAi approach to assess the impact of acute *Nuak1* suppression on pre-existing tumors. We used Villin-CreER[T2] to limit expression of rtTA[3] to the mouse intestine. Upon activation with doxycycline (Dox), rtTA[3] was then used to drive expression of either of 2 shRNAs, targeting *Nuak1* mRNA from nucleotide 612 or 1533 respectively, stringently selected to specifically deplete *Nuak1* as previously described (see Supplementary Methods). Figure S6A shows depletion of NUAK1 in MEFs upon Dox-dependent expression of *Nuak1* shRNA.

Tumors were initiated in heterozygous *floxed Apc* (VA) mice by Tamoxifen-dependent activation of CreER[T2], and tumor development in the colon was accelerated by treatment with dextran sulfate sodium salt (DSS). DSS-treated VA mice develop colonic polyps within 70 days of CreER[T2] activation with >90% penetrance (36), and this time post-induction was chosen to commence Dox-dependent induction of either shRNA. Mice were maintained on Dox for 1 week then harvested for analysis (for a schematic, see Fig. S6B). DSS-treated VA mice lacking either *Nuak1* shRNA or *rtTA* alleles were similarly administered Dox, to control for effects of the antibiotic. Depletion of *Nuak1* for just one week strongly reduced the number of tumors per mouse and moreover suppressed the size of the remaining tumors found upon examination (Fig. 7A). Similar results were obtained with both *Nuak1* shRNA alleles, strongly suggesting that the observed effects reflect the "on-target" depletion of *Nuak1*. Of the tumors that persisted in Nuak1 shRNA-expressing mice, all expressed readily detectable levels of *Nuak1* mRNA, as measured by ISH (Fig. S6C), indicating that some tumors escape shRNA-mediated Nuak1 depletion. PEARL imaging of intestines of mice injected overnight with Licor ROSstar™ reagent revealed elevated ROS levels in colonic tumors *in situ* after just 2 days of NUAK1 depletion (Fig. S6D) while IHC analysis showed increased oxidative damage (8-oxo-dG), increased apoptosis (TUNEL), and reduced proliferation (BrdU) in NUAK1-depleted tumors within the same timeframe (Fig. 7B, C). Consistent with our *in vitro* data, transcriptomic analysis of NUAK1-depleted tumors revealed significantly reduced expression of a host of NRF2 target genes within 2 days of NUAK1 depletion (Fig. S6E). Importantly, exogenous provision of the antioxidant N-Acetyl-Cysteine (NAC) in drinking water reversed the tumor suppressive effect of *Nuak1* depletion (Fig. 7D & S6F), but had no effect on *Nuak1*-replete tumors (Fig. S6G). We conclude from these results that impairment of cellular anti-oxidant defenses is the underlying mechanism of the tumoricidal effect of *Nuak1* suppression in the gut.

Discussion

Here we demonstrate that the AMPK-related kinase NUAK1 plays a key role in protecting colorectal tumors from oxidative stress. Using a combination of genetic and pharmacological approaches, we show that Nuak1 is required for both formation and

maintenance of colorectal tumors after loss of Apc; that suppression of NUAK1 reduces viability of transformed intestinal spheroids and of human colorectal cell lines; and that protecting cells from toxic levels of ROS, via facilitation of NRF2-dependent anti-oxidant gene expression, is a key tumor-promoting activity of NUAK1. We show that NUAK1 kinase activity is rapidly increased by ROS following Cysteine oxidation and, moreover, that NUAK1 is transcriptionally regulated by NRF2, placing NUAK1 squarely within the oxidative stress response pathway. Noting that NUAK1 expression is normally highest in highly oxidative tissues (11) it thus appears that protecting cells from oxidative stress is a major physiological role of NUAK1 that has been co-opted by tumor cells to support their survival in the typically harsh tumor microenvironment. AMPK also participates in antioxidant defense albeit indirectly, by conserving NADPH levels via inhibition of lipid biosynthesis (37), and a recent paper has shown a genetic requirement for this activity in MYC-overexpressing melanoma (38). Although AMPK may under certain circumstances directly phosphorylate NRF2 (27), in our system, the observed level of NRF2 phosphorylation is extremely low and is not modulated by NUAK1 inhibition. As such, AMPK does not presently appear to contribute to regulation of NRF2 by NUAK1.

Instead, we show that NUAK1 facilitates nuclear import of NRF2 by counteracting negative regulation of this process by GSK3β and that direct inhibition of GSK3β restores NRF2 nuclear import in NUAK1-deficient cells. ROS inactivation of PTEN activates AKT, resulting in direct inhibitory phosphorylation of GSK3β on Ser9 (31, 39). This phosphorylation is opposed by PP1β, which reactivates GSK3β (33). We show that activation of AKT by ROS is unaffected by NUAK1 suppression, however, AKT-dependent regulation of GSK3β is facilitated by inhibition of PP1β by NUAK1 via phosphorylation of the PP1β regulatory subunit MYPT1. NUAK1 is thus required to coordinate inhibition of PP1β with AKT activation in response to ROS, thereby allowing GSK3β to be switched off long enough to permit NRF2 nuclear accumulation, providing fascinating new insight into temporal coordination of Redox signal transduction. This role of NUAK1 is likely to be shared with NUAK2, which similarly suppresses PP1β via MYPT1, and indeed, we show that depletion of NUAK2 similarly reduces nuclear NRF2 in cells that highly express NUAK2. However, further work is needed to distinguish between specific effects of NUAK1 and NUAK2 on PP1β and beyond.

This mechanism of regulation suggests that the effects of NUAK1 suppression may be quite pleiotropic and indeed, our phosphor-proteomic analysis indicated modulation of multiple GSK3β targets in addition to NRF2. Moreover, transcriptional regulation by NRF2 reaches far beyond anti-oxidant gene expression, as previously noted (25). However, the central role of NRF2-dependent anti-oxidant gene expression in supporting tumor cell viability is attested to 1) by the hypersensitivity of NUAK1-depleted CRC tumor lines to oxidative stress-induced apoptosis and 2) by the dramatic rescue of NUAK1-depleted colonic tumors and inhibitor-treated spheroids upon provision of exogenous anti-oxidants. The more modest (but nonetheless significant) anti-oxidant rescue observed in HTH-01-015-treated CRC cells likely reflect the limits of trying to buffer against oxidative stress in standard cell culture (40). Although attempts to recapitulate the cytotoxic effects of NUAK1 inhibition in CRC cells using RNAi were unsuccessful, we believe that the effects of HTH-01-015 are specific for NUAK1 for several reasons: 1) This compound has been tested against over 120 kinases

and is extremely selective for NUAK1, although at higher concentrations it does show some activity towards NUAK2 and possibly MARK3 (23); 2) Cytotoxicity was only observed at concentrations that yielded a clear reduction in MYPT1 phosphorylation, thus indicating greater suppression of either NUAK1 or a NUAK1-like activity; 3) cytotoxicity was reproducible with the unrelated compound WZ4003; 4) consistent with our previous demonstration of a synthetic lethal relationship between MYC & NUAK1 (9), sensitivity to HTH-01-015 was MYC-dependent and CRC cell death was rescued by MYC depletion. It is thus unclear why cytotoxicity was not observed using RNAi in the cell culture setting, except in instances of simultaneous peroxide challenge. It maybe that very low levels of residual NUAK1 suffice to suppress cell death, consistent with our data in SW620 cells, which do express very low levels of NUAK1. Additionally, the asynchronous nature of RNAi may allow cultured cell populations time to quench H_2O_2 before the threshold for loss of viability is breached and, accordingly, depletion of NUAK1 resulted in upregulation of NUAK2 in multiple CRC lines, likely dampening the impact of NUAK1 depletion. Furthermore, HTH-01-015 has been shown to partially inhibit NUAK2 at the 10μM dose that exhibited cytotoxicity in CRC lines (23) and, while we cannot entirely exclude the possibility of an off-target effect of the inhibitor, the fact that CRC cytotoxicity at this dose was significantly rescued by both anti-oxidant provision and by depletion of c-MYC strongly supports our interpretation that the on-target effect of the inhibitor is responsible for induction of tumor cell death. The differential sensitivity of some cells (eg. SW480) to the NUAK1 inhibitor versus peroxide challenge after NUAK1 depletion by RNAi may thus reflect expression of NUAK2 and/or the continued biochemical activity of residual levels of NUAK1 after RNAi-mediated depletion.

Our previous work linked the selective requirement of tumor cells for NUAK1 to MYC overexpression, and this link is borne out here by the rescue of NUAK1 inhibitor-induced death upon depletion of MYC from CRC cell lines. In the intestine, loss of *Apc* leads to β-Catenin-dependent overexpression of endogenous Myc. Although deregulated Myc is alone insufficient for intestinal tumor formation (41), it is nonetheless required for β-Catenin-driven polyposis and, significantly, is also required for the elevation of ROS levels observed *in vivo* upon loss of *Apc* (42).

Colorectal tumors will thus have evolved in the face of continuous oxidative stress and cells derived therefrom would likely be better buffered against oxidative stress than cells (eg. U2OS) that lack MYC deregulation. Accordingly we show that U2OS cells depleted of NUAK1 are exquisitely sensitive to a peroxide challenge and that this is phenocopied by MYC overexpression. Note that the absence of NUAK2 expression from U2OS cells likely increases their reliance upon NUAK1. NUAK1 thus functions in 2 major tumor-protective pathways, ATP homeostasis and the oxidative stress response, that are rapidly engaged to support viability upon MYC overexpression (43). As such, NUAK1 appears to be more intimately linked with the downstream metabolic consequences of MYC deregulation than with the absolute levels of MYC protein *per se* and we recently linked MYC deregulation to Calcium-dependent activation of NUAK1 in *LKB1* deficient cells (13).

Exploiting the heightened sensitivity of tumor cells to ROS is emerging as a plausible strategy for cancer therapy (44, 45). Recently, intravenous injection of very high doses of di-

hydro-Ascorbate was shown to suppress colorectal tumor formation by saturating ROS scavengers, and subsequent work suggests that this strategy may indeed show clinical benefit (46, 47). With increasing evidence linking elevated NRF2 to aggressive disease (48, 49), disabling anti-oxidant defenses via transient inhibition of NUAK1 may offer a new strategy for improving therapeutic outcomes in cancer.

Materials & Methods

Mouse experiments and analyses

All experiments involving mice were approved by the local ethics committee and conducted in accordance with UK Home Office license numbers 70/7950 & 70/8646. Mice were housed in a constant 12hr light/dark cycle, and fed and watered ad libitum. Mice bearing doxycycline-inducible shRNAs targeting NUAK1 are described in the supplementary materials section. All mice were maintained on mixed (FVBN x C57Bl/6 x 129/SV) background and littermate controls were used for all experiments. To induce allele recombination, transient activation of CreER^{T2} in the intestine was performed on mice aged 6-12 weeks via single IP injection of 50mg/kg Tamoxifen. For survival analysis, humane end points were defined as exhibition of 2 or more symptoms: >15% weight loss; pale feet; lethargy; bloody stool. Where indicated, 1.75% dextran sodium sulfate (DSS), m.w. 35k-50kDa (M.P. Biochemicals) was administered in drinking water for 5 days, commencing 4 days post allele induction, followed by distilled water for 1 week, then tap water. Doxycycline (Sigma; in H_2O) was administered by oral gavage in 2mg daily boluses, from day 64 to day 70 post-induction. N-Acetyl-Cysteine (Sigma; 4% w/v soln.) was administered in drinking water, starting 3 days before shRNA induction, and replaced every 3-4 days until sacrifice. All mice were sacrificed using a schedule 1 procedure. ROSstar 650 reagent (Licor) was injected IP the day before tissue harvesting and signal was detected by PEARL imaging.

Crypt culture

Primary spheroid cultures of intestinal crypts were established as previously described (50) from the SI and Colon of VA^{Hom}K and VA^{Hom}KN mice: Adult mice were induced as above and tissues harvested 4 days later. Intestines were flushed with ice-cold PBS and opened longitudinally and villi were removed using a glass coverslip. Intestines were incubated in EDTA/PBS (2mM for SI; 25mM for LI) for 30min at 4°C. Excess solution was discarded and loose intestine fragments were collected by manual trituration in 3 PBS washes. The crypt-enriched fractions were passed through a 70μM cell strainer and pelleted at 600rpm for 2min in a table-top centrifuge. Resuspended crypts were counted by hemocytometer, then seeded in Matrigel (BD Bioscience) with Advanced DMEM/F12 media (Invitrogen), supplemented with 10mM HEPES; 2mM Glutamine; 0.1% FBS; Pen/Strep, N-2 & B-27 supplements (1X, Invitrogen). Alternatively, for quantification of primary spheroid formation, isolated crypts were further incubated in Cell Dissociation solution (Thermo) until a single cell suspension was achieved. Cells were then counted and seeded at normalized density as above. Growth factors Noggin (100ng/ml) and EGF (50ng/ml; Peprotech) were added to primary cultures but removed from subsequent passages. Spheroids were counted manually 3 or 4 days after seeding. Wild-type organoid cultures

were prepared similarly but additionally supplemented with R-Spondin (500ng/ml; R&D systems). Established crypt cultures were split 1-2 times per week by manual disruption followed by incubation in Cell Dissociation solution (Thermo) until a single cell suspension was achieved. Cells were then counted and re-seeded at normalized density. NUAK1 inhibitors, HTH-01-015 (Apex Biotech) or WZ4003 (Medchem Express) in DMSO, were added to single cell suspensions at the indicated concentrations. Trolox [(±)-6-Hydroxy-2,5,7,8-tetramethylchromane-2-carboxylic acid] (Sigma) was added to single cell suspensions at a final concentration of 500μM for 16hrs prior to HTH-01-015 and replenished daily for 3 days. ROS detection was performed by confocal fluorescent microscopy using 5μM CellRox green (Thermo; 3hrs @ 37C) after overnight treatment of pre-formed spheroids with HTH-01-015.

Cell Lines

U2OS (2009), HCT116, SW620 & SW480 (all in 2013) cell lines were obtained from the ATCC and cultured in DMEM supplemented with Penn/Strep & 10% FBS. Cells were expanded initially upon receipt and aliquoted into frozen stocks. Upon resuscitation, cells were passaged as required and discarded after no more than 3 months of continuous culture. Cell lines were periodically validated using the Promega Geneprint 10 authentication kit, most recently in August 2017. All cell lines in culture were tested every 3 months for mycoplasma.

Transcriptomic Analysis

Whole-transcriptome analysis was performed by Illumina RNA-Sequencing. The following datasets are available through ArrayExpress: U2OS +/- NUAK1 shRNA, accession number E-MTAB-6244; SW480 +/- siNRF2 or siNUAK1, accession number E-MTAB-6264; *Apc*/DSS-induced colonic tumors +/- shNUAK1, accession number E-MTAB-6265. A full description of methodology is provided in the Supplementary Material.

Statistical Analysis

All experiments were performed at least 3 times except where noted in the text. Raw data obtained from quantitative Real Time PCR, FACS and spheroid generation assays were copied into Excel (Microsoft) or Prism (Graphpad) spreadsheets. All Mean & SEM values of biological replicates were calculated using the calculator function. Graphical representation of such data was also produced in Excel or in Prism. Box & spider plots were generated using Prism. Statistical significance for pairwise data was determined by the Student's (Unpaired) or Paired T test, as indicated. For multiple comparisons, ANOVA was used with a post-hoc Tukey test. * denotes $P<0.05$; ** denotes $P<0.01$; *** denotes $P<0.001$. For Kaplan-Meier plots, Mantel Cox logrank P values are presented; for tumor enumeration, Mann Whitney tests were performed.

Supplementary Material

Refer to Web version on PubMed Central for supplementary material.

Acknowledgements

References

1. Vander Heiden MG, DeBerardinis RJ. Understanding the Intersections between Metabolism and Cancer Biology. Cell. 2017; 168:657–69. [PubMed: 28187287]

2. Sabharwal SS, Schumacker PT. Mitochondrial ROS in cancer: initiators, amplifiers or an Achilles' heel? Nat Rev Cancer. 2014; 14:709–21. [PubMed: 25342630]

3. Lizcano JM, Goransson O, Toth R, Deak M, Morrice NA, Boudeau J, et al. LKB1 is a master kinase that activates 13 kinases of the AMPK subfamily, including MARK/PAR-1. EMBO J. 2004; 23:833–43. [PubMed: 14976552]

4. Bright NJ, Thornton C, Carling D. The regulation and function of mammalian AMPK-related kinases. Acta Physiol (Oxf). 2009; 196:15–26. [PubMed: 19245655]

5. Monteverde T, Muthalagu N, Port J, Murphy DJ. Evidence of cancer-promoting roles for AMPK and related kinases. FEBS J. 2015; 282:4658–71. [PubMed: 26426570]

6. Benaich N, Woodhouse S, Goldie SJ, Mishra A, Quist SR, Watt FM. Rewiring of an epithelial differentiation factor, miR-203, to inhibit human squamous cell carcinoma metastasis. Cell Rep. 2014; 9:104–17. [PubMed: 25284788]

7. Bell RE, Khaled M, Netanely D, Schubert S, Golan T, Buxbaum A, et al. Transcription factor/microRNA axis blocks melanoma invasion program by miR-211 targeting NUAK1. J Invest Dermatol. 2014; 134:441–51. [PubMed: 23934065]

8. Obayashi M, Yoshida M, Tsunematsu T, Ogawa I, Sasahira T, Kuniyasu H, et al. microRNA-203 suppresses invasion and epithelial-mesenchymal transition induction via targeting NUAK1 in head and neck cancer. Oncotarget. 2016; 7:8223–39. [PubMed: 26882562]

9. Liu L, Ulbrich J, Muller J, Wustefeld T, Aeberhard L, Kress TR, et al. Deregulated MYC expression induces dependence upon AMPK-related kinase 5. Nature. 2012; 483:608–12. [PubMed: 22460906]

10. Zagorska A, Deak M, Campbell DG, Banerjee S, Hirano M, Aizawa S, et al. New roles for the LKB1-NUAK pathway in controlling myosin phosphatase complexes and cell adhesion. Sci Signal. 2010; 3:ra25. [PubMed: 20354225]

11. Inazuka F, Sugiyama N, Tomita M, Abe T, Shioi G, Esumi H. Muscle-specific knock-out of NUAK family SNF1-like kinase 1 (NUAK1) prevents high fat diet-induced glucose intolerance. J Biol Chem. 2012; 287:16379–89. [PubMed: 22418434]

12. Suzuki A, Kusakai G, Kishimoto A, Lu J, Ogura T, Esumi H. ARK5 suppresses the cell death induced by nutrient starvation and death receptors via inhibition of caspase 8 activation, but not by chemotherapeutic agents or UV irradiation. Oncogene. 2003; 22:6177–82. [PubMed: 13679856]

13. Monteverde T, Tait-Mulder J, Hedley A, Knight JR, Sansom OJ, Murphy DJ. Calcium signalling links MYC to NUAK1. Oncogene. 2017

14. Shaw RJ, Kosmatka M, Bardeesy N, Hurley RL, Witters LA, DePinho RA, et al. The tumor suppressor LKB1 kinase directly activates AMP-activated kinase and regulates apoptosis in response to energy stress. Proc Natl Acad Sci U S A. 2004; 101:3329–35. [PubMed: 14985505]

15. Gwinn DM, Shackelford DB, Egan DF, Mihaylova MM, Mery A, Vasquez DS, et al. AMPK phosphorylation of raptor mediates a metabolic checkpoint. Mol Cell. 2008; 30:214–26. [PubMed: 18439900]

16. Vincent EE, Coelho PP, Blagih J, Griss T, Viollet B, Jones RG. Differential effects of AMPK agonists on cell growth and metabolism. Oncogene. 2015; 34:3627–39. [PubMed: 25241895]

17. Sansom OJ, Meniel VS, Muncan V, Phesse TJ, Wilkins JA, Reed KR, et al. Myc deletion rescues Apc deficiency in the small intestine. Nature. 2007; 446:676–9. [PubMed: 17377531]

18. Cancer Genome Atlas N. Comprehensive molecular characterization of human colon and rectal cancer. Nature. 2012; 487:330–7. [PubMed: 22810696]

19. Myant KB, Cammareri P, McGhee EJ, Ridgway RA, Huels DJ, Cordero JB, et al. ROS production and NF-kappaB activation triggered by RAC1 facilitate WNT-driven intestinal stem cell proliferation and colorectal cancer initiation. Cell Stem Cell. 2013; 12:761–73. [PubMed: 23665120]

20. Aguirre-Gamboa R, Gomez-Rueda H, Martinez-Ledesma E, Martinez-Torteya A, Chacolla-Huaringa R, Rodriguez-Barrientos A, et al. SurvExpress: an online biomarker validation tool and database for cancer gene expression data using survival analysis. PLoS One. 2013; 8:e74250. [PubMed: 24066126]

21. Smith JJ, Deane NG, Dhawan P, Beauchamp RD. Regulation of metastasis in colorectal adenocarcinoma: a collision between development and tumor biology. Surgery. 2008; 144:353–66. [PubMed: 18707034]

22. Jorissen RN, Gibbs P, Christie M, Prakash S, Lipton L, Desai J, et al. Metastasis-Associated Gene Expression Changes Predict Poor Outcomes in Patients with Dukes Stage B and C Colorectal Cancer. Clin Cancer Res. 2009; 15:7642–51. [PubMed: 19996206]

23. Banerjee S, Buhrlage SJ, Huang HT, Deng X, Zhou W, Wang J, et al. Characterization of WZ4003 and HTH-01-015 as selective inhibitors of the LKB1-tumour-suppressor-activated NUAK kinases. Biochem J. 2014; 457:215–25. [PubMed: 24171924]

24. Schwitalla S, Fingerle AA, Cammareri P, Nebelsiek T, Goktuna SI, Ziegler PK, et al. Intestinal tumorigenesis initiated by dedifferentiation and acquisition of stem-cell-like properties. Cell. 2013; 152:25–38. [PubMed: 23273993]

25. Malhotra D, Portales-Casamar E, Singh A, Srivastava S, Arenillas D, Happel C, et al. Global mapping of binding sites for Nrf2 identifies novel targets in cell survival response through ChIP-Seq profiling and network analysis. Nucleic Acids Res. 2010; 38:5718–34. [PubMed: 20460467]

26. Izreig S, Samborska B, Johnson RM, Sergushichev A, Ma EH, Lussier C, et al. The miR-17 approximately 92 microRNA Cluster Is a Global Regulator of Tumor Metabolism. Cell Rep. 2016; 16:1915–28. [PubMed: 27498867]

27. Joo MS, Kim WD, Lee KY, Kim JH, Koo JH, Kim SG. AMPK Facilitates Nuclear Accumulation of Nrf2 by Phosphorylating at Serine 550. Mol Cell Biol. 2016; 36:1931–42. [PubMed: 27161318]

28. Itoh K, Wakabayashi N, Katoh Y, Ishii T, Igarashi K, Engel JD, et al. Keap1 represses nuclear activation of antioxidant responsive elements by Nrf2 through binding to the amino-terminal Neh2 domain. Genes Dev. 1999; 13:76–86. [PubMed: 9887101]

29. McMahon M, Itoh K, Yamamoto M, Hayes JD. Keap1-dependent proteasomal degradation of transcription factor Nrf2 contributes to the negative regulation of antioxidant response element-driven gene expression. J Biol Chem. 2003; 278:21592–600. [PubMed: 12682069]

30. Dinkova-Kostova AT, Holtzclaw WD, Cole RN, Itoh K, Wakabayashi N, Katoh Y, et al. Direct evidence that sulfhydryl groups of Keap1 are the sensors regulating induction of phase 2 enzymes that protect against carcinogens and oxidants. Proc Natl Acad Sci U S A. 2002; 99:11908–13. [PubMed: 12193649]

31. Rojo AI, Sagarra MR, Cuadrado A. GSK-3beta down-regulates the transcription factor Nrf2 after oxidant damage: relevance to exposure of neuronal cells to oxidative stress. J Neurochem. 2008; 105:192–202. [PubMed: 18005231]

32. Hernandez F, Langa E, Cuadros R, Avila J, Villanueva N. Regulation of GSK3 isoforms by phosphatases PP1 and PP2A. Mol Cell Biochem. 2010; 344:211–5. [PubMed: 20652371]

33. Mobasher MA, Gonzalez-Rodriguez A, Santamaria B, Ramos S, Martin MA, Goya L, et al. Protein tyrosine phosphatase 1B modulates GSK3beta/Nrf2 and IGFIR signaling pathways in acetaminophen-induced hepatotoxicity. Cell Death Dis. 2013; 4:e626. [PubMed: 23661004]

34. Sullivan LB, Chandel NS. Mitochondrial reactive oxygen species and cancer. Cancer Metab. 2014; 2:17. [PubMed: 25671107]

35. Seo YH, Carroll KS. Profiling protein thiol oxidation in tumor cells using sulfenic acid-specific antibodies. Proc Natl Acad Sci U S A. 2009; 106:16163–8. [PubMed: 19805274]

36. Tanaka T, Kohno H, Suzuki R, Hata K, Sugie S, Niho N, et al. Dextran sodium sulfate strongly promotes colorectal carcinogenesis in Apc(Min/+) mice: inflammatory stimuli by dextran sodium sulfate results in development of multiple colonic neoplasms. Int J Cancer. 2006; 118:25–34. [PubMed: 16049979]

37. Jeon SM, Chandel NS, Hay N. AMPK regulates NADPH homeostasis to promote tumour cell survival during energy stress. Nature. 2012; 485:661–5. [PubMed: 22660331]

38. Kfoury A, Armaro M, Collodet C, Sordet-Dessimoz J, Giner MP, Christen S, et al. AMPK promotes survival of c-Myc-positive melanoma cells by suppressing oxidative stress. EMBO J. 2018

39. Lee SR, Yang KS, Kwon J, Lee C, Jeong W, Rhee SG. Reversible inactivation of the tumor suppressor PTEN by H2O2. J Biol Chem. 2002; 277:20336–42. [PubMed: 11916965]

40. Parrinello S, Samper E, Krtolica A, Goldstein J, Melov S, Campisi J. Oxygen sensitivity severely limits the replicative lifespan of murine fibroblasts. Nat Cell Biol. 2003; 5:741–7. [PubMed: 12855956]

41. Finch AJ, Soucek L, Junttila MR, Swigart LB, Evan GI. Acute overexpression of Myc in intestinal epithelium recapitulates some but not all the changes elicited by Wnt/beta-catenin pathway activation. Mol Cell Biol. 2009; 29:5306–15. [PubMed: 19635809]

42. Cheung EC, Lee P, Ceteci F, Nixon C, Blyth K, Sansom OJ, et al. Opposing effects of TIGAR- and RAC1-derived ROS on Wnt-driven proliferation in the mouse intestine. Genes Dev. 2016; 30:52–63. [PubMed: 26679840]

43. Stine ZE, Walton ZE, Altman BJ, Hsieh AL, Dang CV. MYC, Metabolism, and Cancer. Cancer Discov. 2015; 5:1024–39. [PubMed: 26382145]

44. Raj L, Ide T, Gurkar AU, Foley M, Schenone M, Li X, et al. Selective killing of cancer cells by a small molecule targeting the stress response to ROS. Nature. 2011; 475:231–4. [PubMed: 21753854]

45. Gorrini C, Harris IS, Mak TW. Modulation of oxidative stress as an anticancer strategy. Nat Rev Drug Discov. 2013; 12:931–47. [PubMed: 24287781]

46. Yun J, Mullarky E, Lu C, Bosch KN, Kavalier A, Rivera K, et al. Vitamin C selectively kills KRAS and BRAF mutant colorectal cancer cells by targeting GAPDH. Science. 2015; 350:1391–6. [PubMed: 26541605]

47. Schoenfeld JD, Sibenaller ZA, Mapuskar KA, Wagner BA, Cramer-Morales KL, Furqan M, et al. O2- and H2O2-Mediated Disruption of Fe Metabolism Causes the Differential Susceptibility of NSCLC and GBM Cancer Cells to Pharmacological Ascorbate. Cancer Cell. 2017; 31:487–500 e8. [PubMed: 28366679]

48. DeNicola GM, Karreth FA, Humpton TJ, Gopinathan A, Wei C, Frese K, et al. Oncogene-induced Nrf2 transcription promotes ROS detoxification and tumorigenesis. Nature. 2011; 475:106–9. [PubMed: 21734707]

49. Chio IIC, Jafarnejad SM, Ponz-Sarvise M, Park Y, Rivera K, Palm W, et al. NRF2 Promotes Tumor Maintenance by Modulating mRNA Translation in Pancreatic Cancer. Cell. 2016; 166:963–76. [PubMed: 27477511]

50. Sato T, Vries RG, Snippert HJ, van de Wetering M, Barker N, Stange DE, et al. Single Lgr5 stem cells build crypt-villus structures in vitro without a mesenchymal niche. Nature. 2009; 459:262–5. [PubMed: 19329995]

Significance

This work identifies NUAK1 as a key facilitator of the adaptive anti-oxidant response that is associated with aggressive disease and worse outcome in human CRC. Our data suggest that transient NUAK1 inhibition may provide a safe and effective means for treatment of human CRC via disruption of intrinsic anti-oxidant defences.
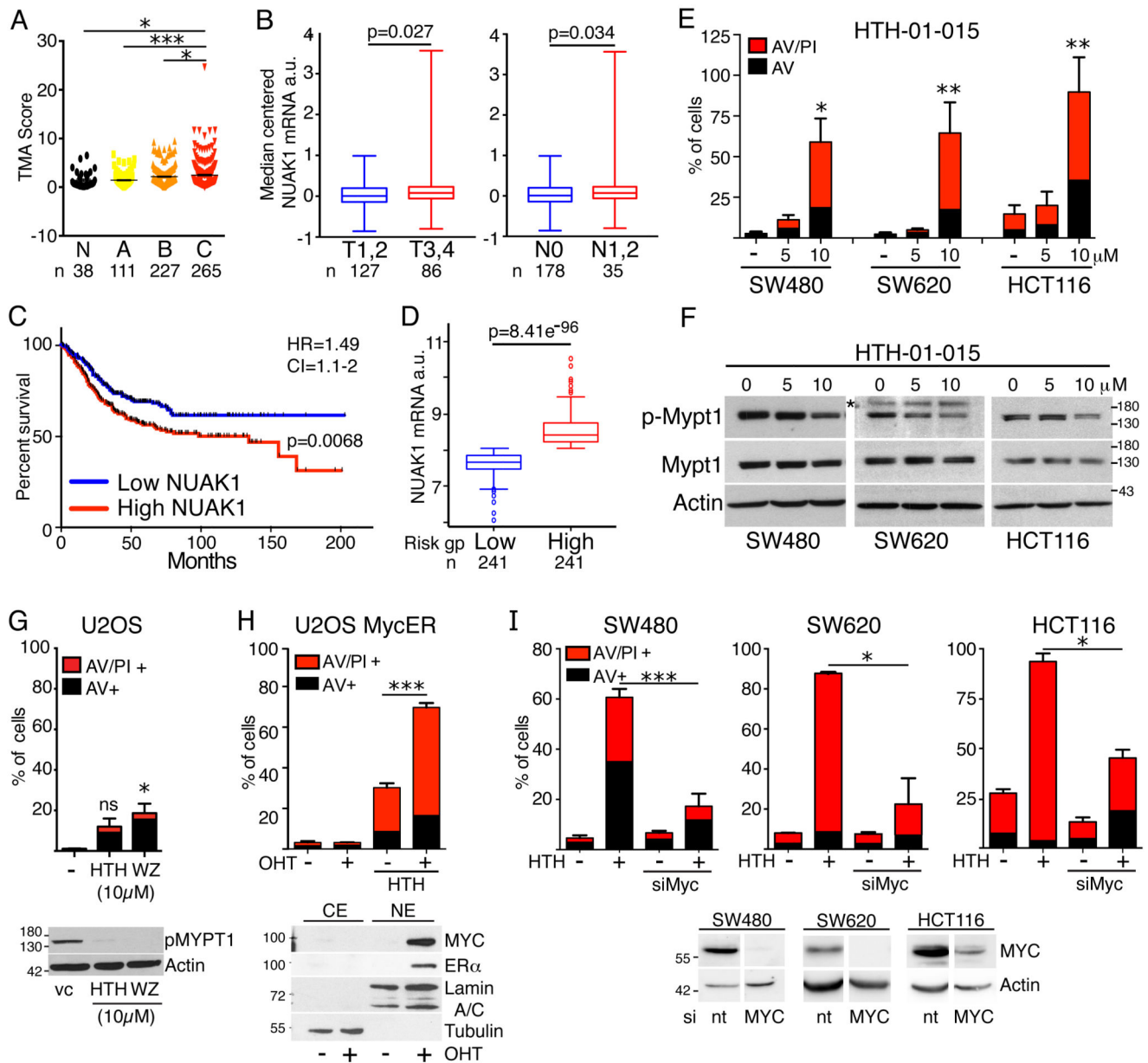
Figure 1. NUAK1 overexpression correlates with tumor progression, lymph node infiltrates, and reduced OS in human CRC

A) Summary of *NUAK1* mRNA detection in a human CRC TMA (N=660), sorted by Dukes' grade A-C; N=normal colon. Asterisks indicate significance (1-way ANOVA & post-hoc Tukey test). **B)** Box and whisker plots of median-centered NUAK1 mRNA expression from the TCGA colorectal adenocarcinoma cohort accessed via Oncomine: Left panel shows early (T1,2) versus late (T3, 4) stage CRC; right panel shows tumors with (N1,2) or without (N0 lymph node metastasis. **C)** Overall survival of human CRC patients (N=947) separated by high versus low *NUAK1* expression. Logrank P value, hazard ratio (HR) and 95% confidence interval (CI) shown. **D)** Box & whisker plots of NUAK1 mRNA levels in human CRC separated by risk group as per (C). T-test P value shown. (C&D) Data were mined and

graphs adapted from Metabase SurvExpress. **E)** Apoptosis induced in human CRC cell lines 48hrs after treatment with the indicated concentrations of HTH-01-015. Red bars indicate AnnexinV/Propidium Iodide (AV/PI) double positive cells; black bars indicate AnnexinV positive cells. Mean and SEM of 3 independent experiments shown; asterisks show significance (ANOVA & post-hoc Tukey test, relative to vehicle treated controls (-)). **F)** Immunoblots of lysates from human CRC cell lines show reduction in MYPT1 Ser445 phosphorylation upon inhibition of NUAK1 (8hr). The asterisk indicates a non-specific band. **G)** Apoptosis induced in U2OS cells 48hrs after treatment with 10μM HTH-01-015 or WZ4003. Mean and SEM of 3 independent experiments shown; asterisks show significance (ANOVA & post-hoc Tukey test, relative to vc controls). Ns = not significantly increased relative to untreated controls. Immunoblot (lower panel) shows suppression of p-MYPT1^{S445} upon NUAK1 inhibition. **H)** Apoptosis induced in U2OS-MycER cells upon NUAK1 inhibition in the presence (+ OHT) or absence (- OHT) of 4-hydroxy-tamoxifen-dependent activation of overexpressed MycER. Mean and SEM of 3 independent experiments shown; asterisks denote significance (2-way ANOVA & post-hoc Tukey test). Immunoblot shows nuclear stabilization of MycER by 4-OHT. **I)** Rescue of CRC cells from HTH-01-015-induced apoptosis upon depletion of MYC. Mean and SEM of a representative experiment (N 2) in each cell line shown; asterisks denote significance (ANOVA & post-hoc Tukey test. Immunoblots show depletion of MYC in the same cell lines (lower panels).
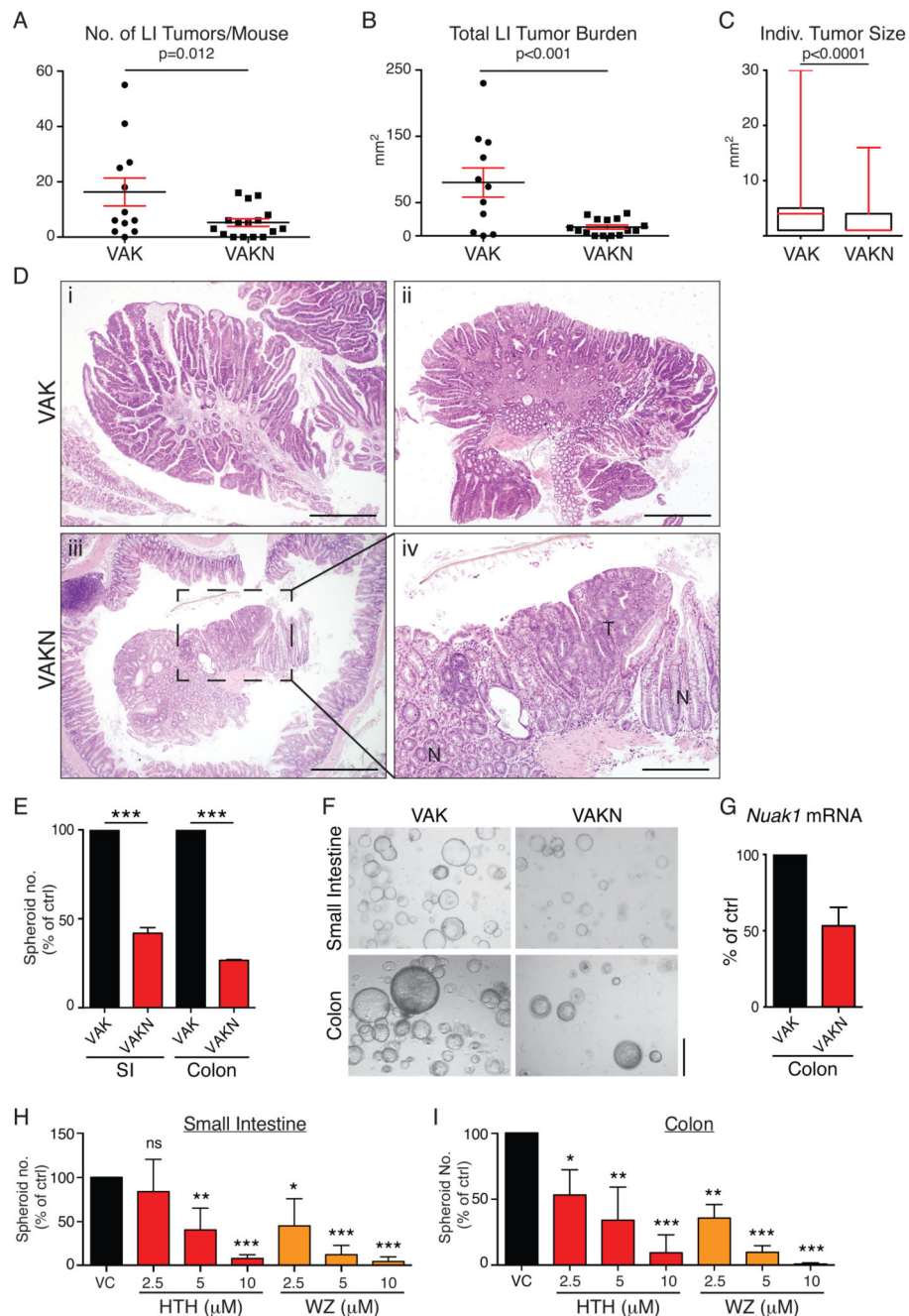
Figure 2. Deletion of Nuak1 suppresses colorectal tumor formation

A) Number of large intestine (LI) tumors per mouse in VAK (N=12) and VAKN (N=16) mice, harvested at end-point. Black bar indicates Mean tumor number while red bars indicate SEM. **B)** Total tumor burden (area) per mouse of the indicated genotypes. Mean & SEM shown. **C)** Size of individual tumors in mice of the indicated genotypes. Box plots depict the median (red bar) and interquartile range of individual tumor area; whiskers reflect maximum observed tumor size. N=192 (VAK) & 119 (VAKN). (A-C) P values from Mann-Whitney test shown. **D)** Representative H&E stained images of tumors from VAK (top

panels) and VAKN (lower panels) mice. Panels i-iii: scale bar =500μm. Panel iv: zoom of inset from iii, scale bar =200μm, T=tumor, N=normal tissue. **E)** Number of spheroids arising from freshly isolated VA^{Hom}KN small and large intestine, normalized to VA^{Hom}K controls seeded on the same day. Mean and SEM from VA^{Hom}K (N=4) and VA^{Hom}KN (N=6) mice shown. *** denotes significance (Unpaired T-test). **F)** Representative images of spheroids from (E). Scale bar =500μm. **G)** Detection of Nuak1 mRNA in colonic spheroids from VA^{Hom}KN mice relative to Nuak1 transcript levels in VAK spheroids. Mean of 4 VA^{Hom}K and 6 VA^{Hom}KN mice shown. Error bar indicates SEM. **H)** Numbers of VA^{Hom}K small intestine-derived spheroids after treatment with Nuak1 inhibitors HTH-01-015 (HTH) or WZ4003 (WZ), normalized to vehicle treated control (vc). Mean & SEM of 3 independent experiments shown; asterisks show significance (1-way ANOVA & post-hoc Tukey test, relative to vc controls). **I)** Numbers of VA^{Hom}K large intestine-derived spheroids treated and graphed as per (H).
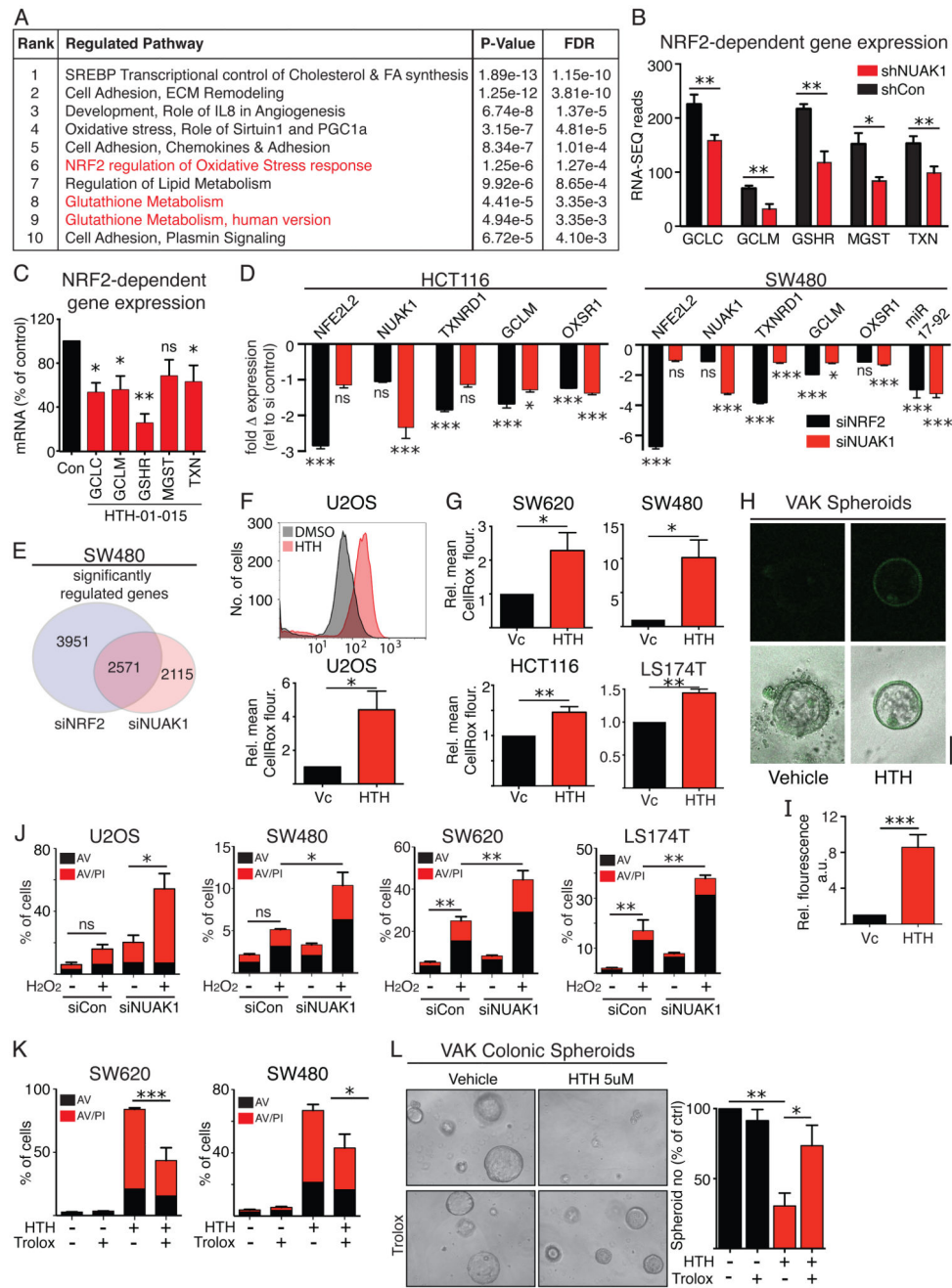
Figure 3. NUAK1 promotes NRF2-dependent gene expression
A) Top 10 pathways modulated in U2OS cells after depletion of NUAK1 by shRNA, identified by Metacore GeneGO analysis of RNA-Seq data. FDR = False discovery rate. **B)** RNA-Seq read counts of select NRF2 targets from (A). Mean & SEM of 3 biological replicates shown; asterisks denote significance (unpaired T-test). **C)** Reduction of NRF2 target gene expression upon inhibition of NUAK1 for 8hrs in U2OS cells. Mean & SEM of 3 independent experiments shown; asterisks denote significance (1-tailed T test). **D)** Comparison of selected NRF2 target gene expression upon depletion of NRF2 versus

depletion of NUAK1 in CRC cell lines, HCT116 and SW480. N=4. Mean & SEM shown; asterisks denote significance (Unpaired T-test). **E)** Global analysis of the transcriptomic impact of NRF2 depletion versus NUAK1 depletion in SW480 cells. **F)** FACS detection of cytosolic ROS levels by CellRox Deep Red™ staining of U2OS cells upon acute inhibition of NUAK1. The upper panel shows a representative FACS graph; the lower panel shows Mean ± SEM fluorescence intensity of HTH-treated relative to vehicle treated control cells from 3 independent experiments. **G)** CellRox detection of ROS levels in human CRC lines, as per (F), upon acute inhibition of NUAK1. Mean ± SEM from 3 independent experiments shown; asterisks denote significance (1-tailed T-test) **H)** Representative image showing CellRox staining of VAK spheroids after treatment with HTH-01-015. **I)** quantification of spheroid fluorescence from (H) using ImageJ. N=41 per group. **J)** Apoptosis induced by treatment of U2OS (500μM) or CRC cells (1mM) with H_2O_2, with and without prior depletion of NUAK1, measured at 24hrs. Mean & SEM of 3 biological replicates from at least 2 independent experiments for each cell line shown. Asterisks denote significance (unpaired T-test). **K)** Provision of exogenous antioxidant Trolox attenuates HTH-01-015-induced killing in human CRC lines. Mean & SEM of 3 independent experiments shown. Asterisks denote significance (2-way ANOVA & post-hoc Tukey test). **L)** Representative images showing Trolox rescues growth of Colonic VA^{Hom}K spheroids from Nuak1 inhibition (3 days). Scale bar =100μm. Right panel shows quantification of spheroids after NUAK1 inhibition in the presence and absence of Trolox (500μM). Mean and SEM of 3 independent experiments, normalized to vehicle treated controls are shown. Asterisks denote significance (2-way ANOVA & post-hoc Tukey test).
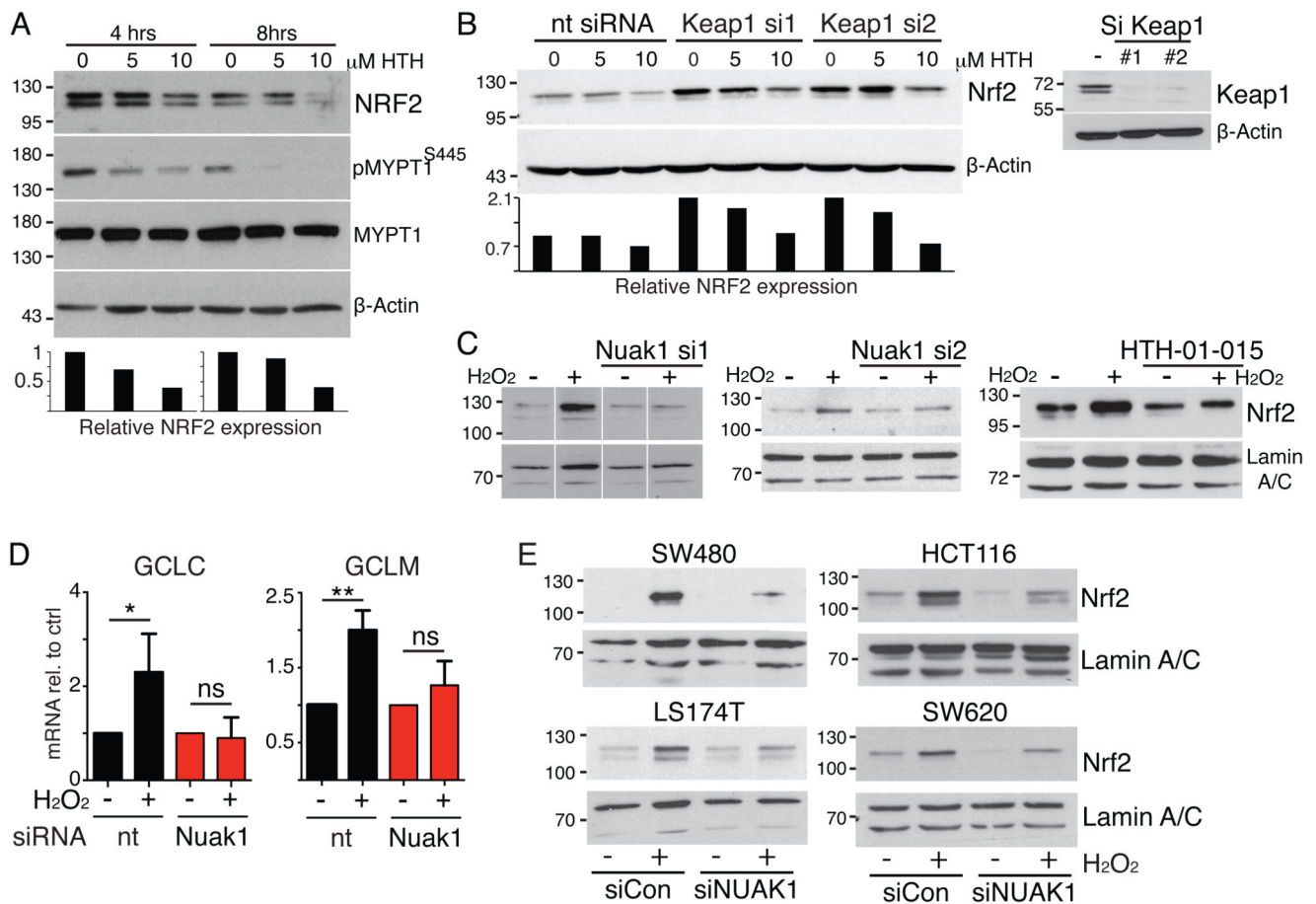
Figure 4. NUAK1 promotes nuclear accumulation of NRF2

A) NRF2 immunoblot of U2OS whole cell extracts harvested after 4 or 8hrs NUAK1 inhibition. Reduced phospo-MYPT1 confirms NUAK1 inhibition. The lower panel shows densitometry of the NRF2 blot shown. **B)** NRF2 immunoblot of KEAP1 depleted U2OS cells upon NUAK1 inhibition for 8hrs. The lower panel shows densitometry of the NRF2 blot shown. The right panel confirms KEAP1 depletion with 2 independent siRNAs. **C)** Immunoblots of NRF2 protein levels in nuclear extracts from U2OS cells after acute (30mins) treatment of cells with $500\mu M$ H_2O_2, with and without prior depletion of NUAK1 by 2 distinct siRNAs (left & center panels), or upon NUAK1 inhibition by HTH-01-015 ($10\mu M$). All blots (A-C) are representative of at least 3 independent experiments. **D)** Expression analysis of NRF2 target genes GCLC and GCLM shows suppression of H_2O_2-induced mRNA levels upon depletion of NUAK1. Mean and SEM of 3 independent experiments, normalized to pre-peroxide treatment, are shown. Asterisks denote significance (2-way ANOVA & post-hoc Tukey test). **E)** Suppression of ROS-induced NRF2 nuclear translocation in multiple human CRC cell lines upon depletion of NUAK1.
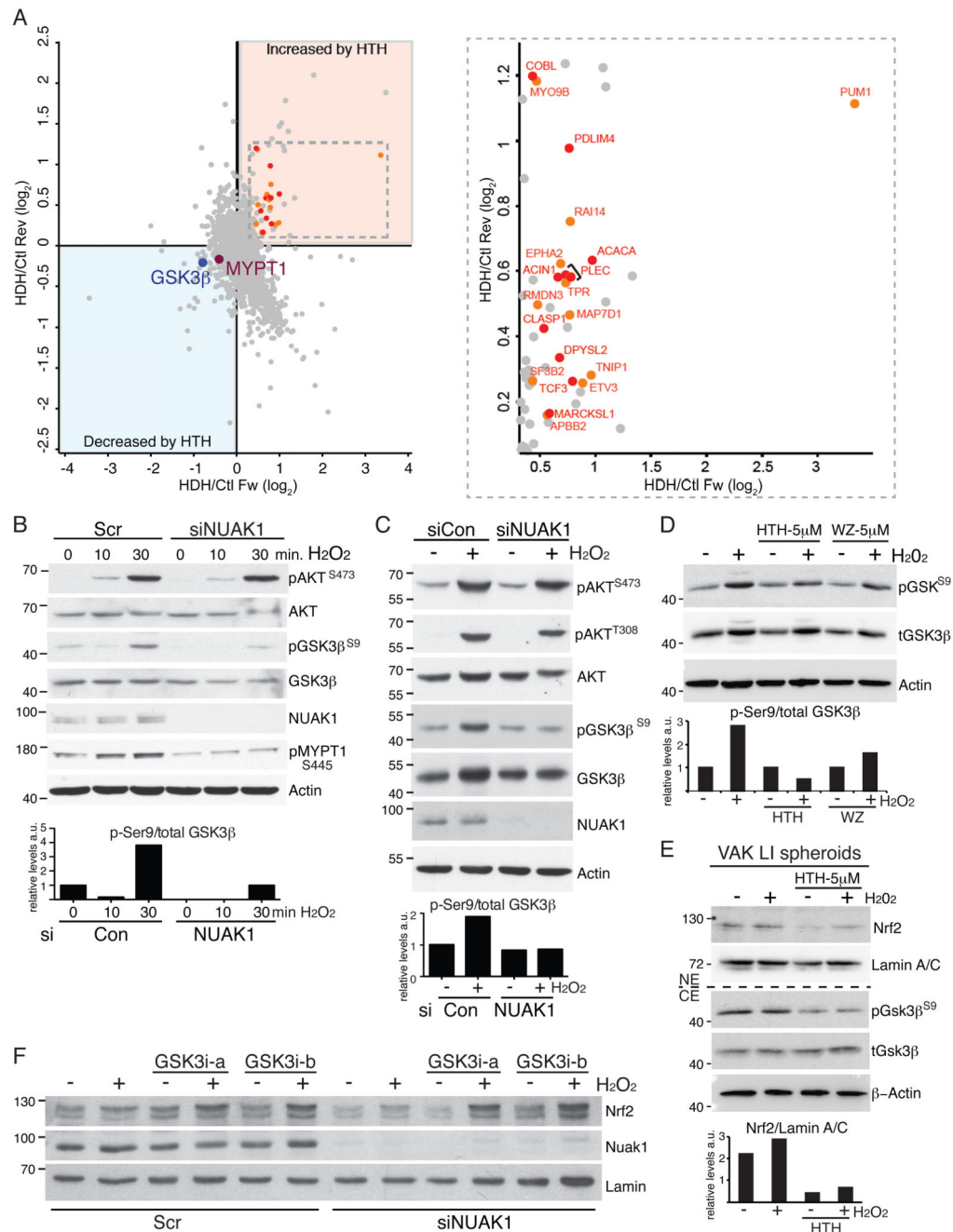
Figure 5. NUAK1 inhibits negative regulation of NRF2 by GSK3β

A) Summary of phospho-proteomic changes induced in U2OS cells upon treatment with 10μM HTH-01-015 for 1hr. Left panel depicts the comparison of "forward" (X-axis) with "reverse" (Y-axis) SILAC labeled cells. Phosphorylation sites in the lower left quadrant thus show consistent reduction in levels while those in the upper right quadrant show consistently higher phosphorylation levels detected by mass spectrometry. The previously validated NUAK1 substrate MYPT1 was used to set a threshold for acceptance/rejection of modulated phosphor-peptides. Right panel shows zoom of the inset from left panel, with known (red)

and predicted (orange) GSK3β substrates highlighted. **B)** Immunoblots of lysates from NUAK1-depleted or control U2OS cells after treatment with H_2O_2 (500μM) showing effects on AKT, GSK3β and MYPT1 phosphorylation. The lower panel shows the ratio of Ser9-phospho-/total GSK3β, measured by Image-J analysis of the presented immunoblots. **C)** Immunoblots of NUAK1-depleted or control SW480 cytosolic fractions after treatment with H_2O_2 (30 minutes). The lower panel shows the ratio of Ser9-phospho-/total GSK3β, measured by Image-J analysis of the presented immunoblots. **D)** Immunoblots show reduced Ser9-phosphorylation of GSK3β in the presence of NUAK1 inhibitors. The lower panel shows the ratio of Ser9-phospho-/total GSK3β, measured by Image-J analysis of the presented immunoblots. **E)** Immunoblots show suppression of nuclear NRF2 and Ser9-phosphorylation of GSK3β upon inhibition of NUAK1 (5μM HTH-01-015 for 16hrs) in VAK large intestine-derived spheroids. Note that the presence of Matrigel likely blunts the impact of treatment with exogenous H_2O_2 (2mM for 1hr). The lower panel shows quantification of nuclear NRF2 levels by Image-J analysis. **F)** Pre-treatment of NUAK1 depleted SW480 cells with GSK3β inhibitors BIO-acetoxime (a; 1μM for 6hrs) or CHIR99021 (b; 3μM for 6hrs) restores ROS-induced NRF2 nuclear translocation. All images are representative of at least 3 independent experiments.
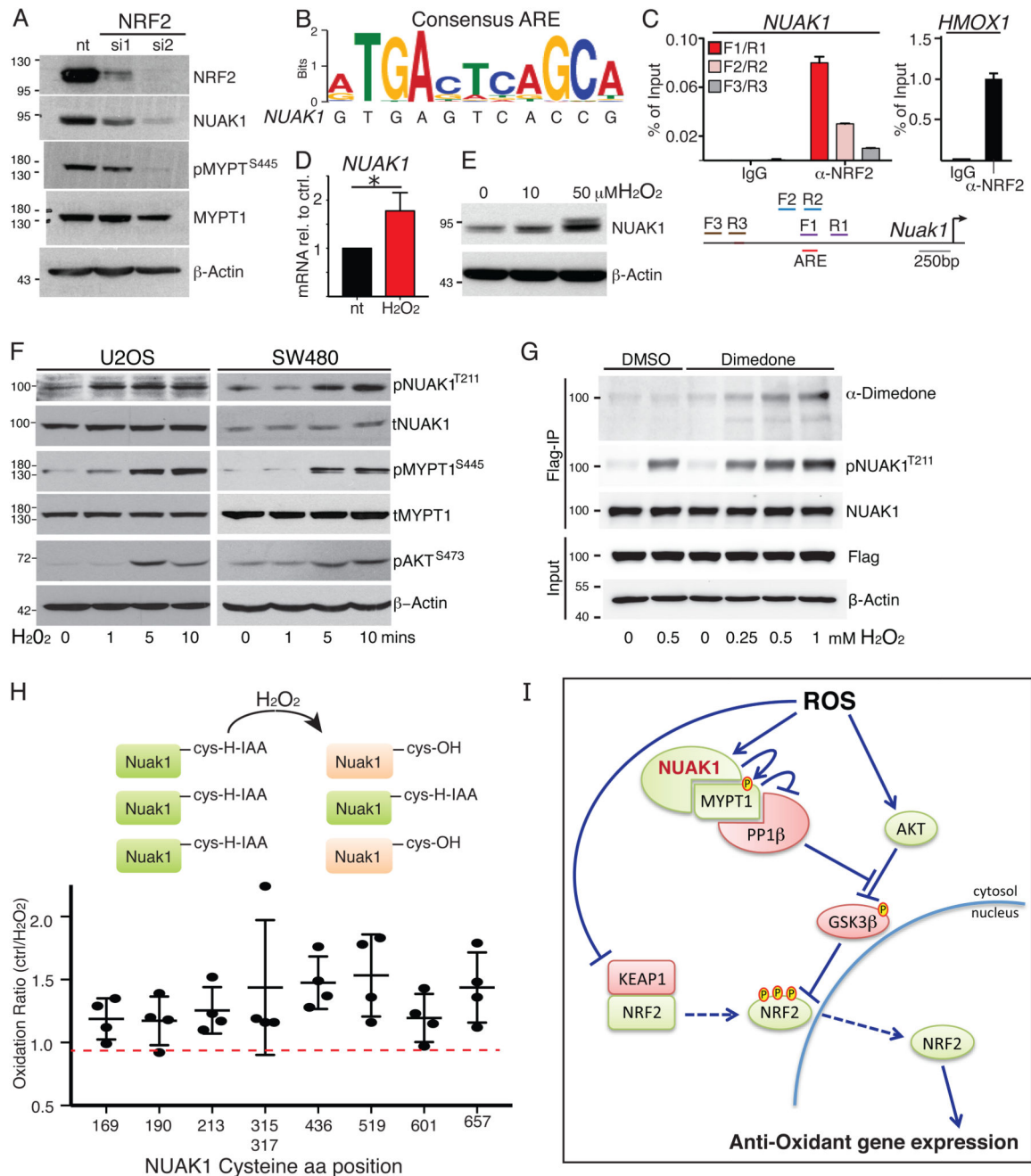
Figure 6. Regulation of NUAK1 by NRF2 and ROS

A) Immunoblots show reduced NUAK1 protein and reduced MYPT1^{S445}-phosphorylation in U2OS cells upon depletion of NRF2 using 2 distinct siRNAs. **B)** Alignment of a putative anti-oxidant response element (ARE) in the NUAK1 promoter with the NRF2-binding consensus sequence. **C)** Chromatin IP of NRF2-bound DNA probed with primer pairs flanking (F1/R1; F2/R2) or distal to (F3/R3) the putative ARE in the NUAK1 promoter (see diagram). The right panel shows NRF2 binding to the canonical target gene HMOX1 from the same analysis. Mean & SEM of technical replicates from 1 of 2 independent experiments

shown. **D)** QPCR measurement of NUAK1 mRNA in U2OS cells treated with/without H_2O_2 (100μM) for 4hrs. Mean & SEM of 3 experiments. * denotes significance (paired T-test). **E)** Immunoblot of NUAK1 protein levels after treatment of U2OS cells (1hr) with the indicated concentrations of H_2O_2. **F)** Immunoblots of T211 NUAK1 and S445 MYPT1 phosphorylation upon acute treatment of U2OS (left panels) or SW480 (right panels) with H_2O_2 for the indicated times. **G)** Oxidation of NUAK1 protein detected by Dimedone labeling of U2OS cells expressing FLAG-tagged NUAK1 and treated for 5 minutes with 500mM H_2O_2. **H)** Identification of oxidized Cysteines in FLAG-tagged NUAK1 by MS analysis of Iodoacetamide labeling of U2OS-FLAG-NUAK1 cells treated with/without H_2O_2 for 5 minutes. Lysates were labeled with heavy (^{13}C) or light (^{12}C) Iodoacetamide, followed by immunoprecipitation of FLAG-NUAK1. Plot shows analysis of reciprocally labeled samples from 2 independent experiments. Mean and SD indicated. **I)** Model integrating NUAK1 suppression of PP1β-dependent de-phosphorylation of GSK3β as an integral step in nuclear mobilization of NRF2 in response to oxidative stress.
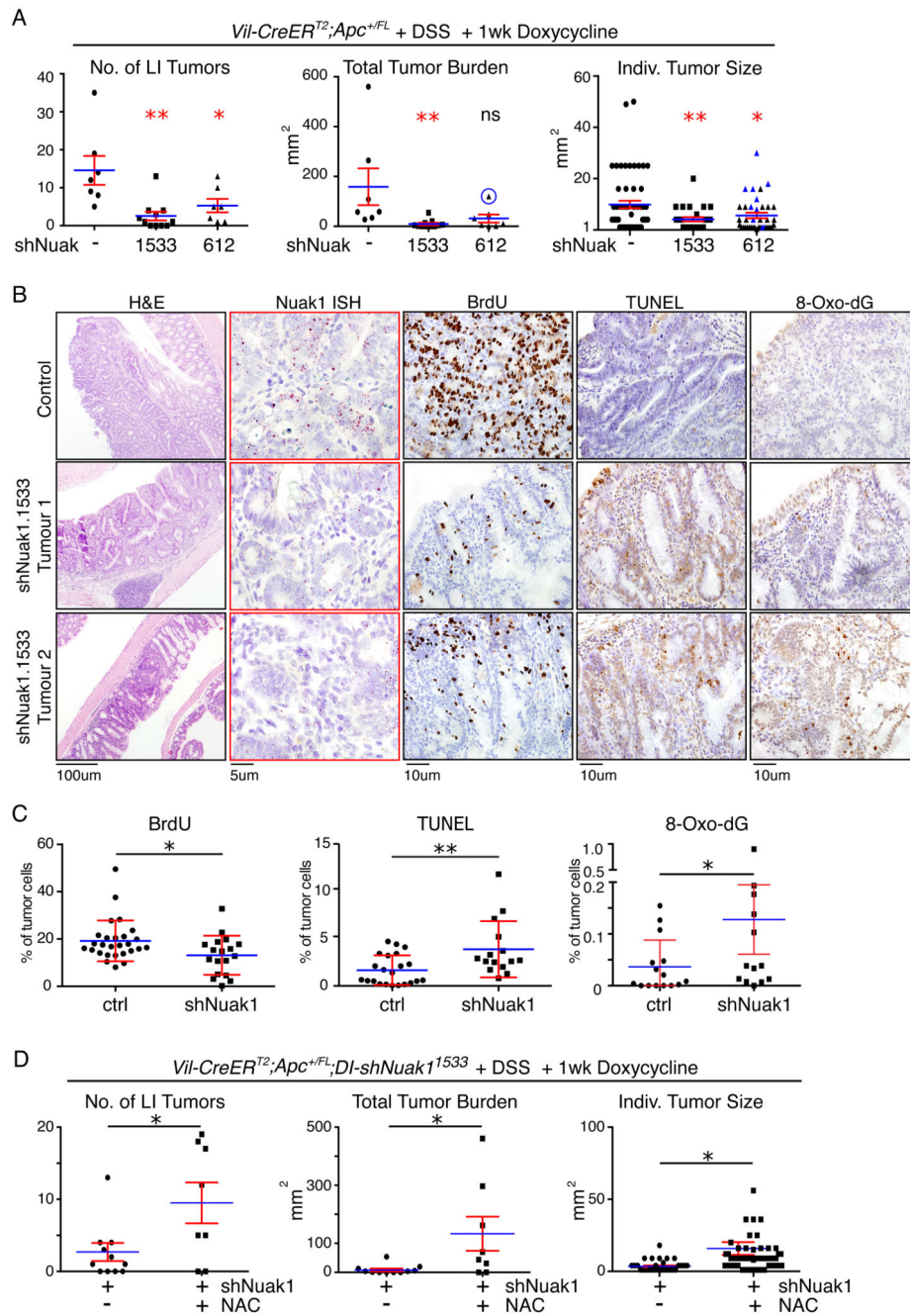

Figure 7. Acute depletion of NUAK1 reverses colorectal tumors via increased ROS

A) Colonic tumor number per mouse (left panel), total tumor burden (center panel) and individual tumor size (right panel), in DSS-treated VA mice after 7 days of Nuak1 depletion in the gut using either of 2 doxycycline-inducible shRNAs (1533, N=10; or 612, N=7), compared with doxycycline treated controls lacking either shRNA or the rtTA3 allele (-, N=7). Graphs depict Mean (blue lines) and SEM (red bars). Red asterisks indicate significance, relative to untreated controls (1-way ANOVA & post-hoc Tukey test). An outlier mouse in the shNuak-612 cohort is circled (center panel) and all tumors present

within the LI of that mouse are labeled in blue (right panel). The outlier and corresponding tumors were included in the statistical analysis. Total tumor burden is significantly reduce by shNUAK1-612 if the outlier is omitted. **B)** Representative IHC analysis of proliferation (BrdU), apoptosis (TUNEL) and oxidative damage (nuclear 8-Oxo-deoxyGuanine) with corresponding ISH analysis of NUAK1 mRNA (red dots) in selected tumors from control (top panels) and shNUAK1-1533 mice treated for 2 days with doxycycline. **C)** HALO automated quantification of BrdU, TUNEL & 8-Oxo-Guanine IHC in individual tumors from shNUAK1 expressing (N=6) or control (N=6) mice, as per (B). Mean (blue bars) and SEM (red bars) indicated. Red asterisks indicate significance (Mann Whitney Test). **D)** Tumor number, total tumor burden and individual tumor size in DSS-treated VA mice after 7 days of Nuak1 depletion in the gut using shNuak-1533, in mice given N-Acetyl-Cysteine (NAC, N=8) compared with no exogenous anti-oxidant (nt). Note that the NAC-untreated data are the same used in (A). Red asterisks indicate significance (Mann Whitney Test).